

Büttiker probes for dissipative phonon quantum transport in semiconductor nanostructures

K. Y. Miao,^{1,2} S. Sadasivam,³ J. Charles,^{1,2} G. Klimeck,^{1,2} T. S. Fisher,³ T. Kubis²

¹*Department of Electrical and Computer Engineering, Purdue University, West Lafayette, Indiana 47907, USA*

²*Network for Computational Nanotechnology, Purdue University, West Lafayette, Indiana 47907, USA*

³*Department of Mechanical Engineering and Birck Nanotechnology Center, Purdue University, West Lafayette, Indiana 47906, USA*

Theoretical prediction of phonon transport in modern semiconductor nanodevices requires atomic resolution of device features and quantum transport models covering coherent and incoherent effects. The nonequilibrium Green's function method (NEGF) is known to serve this purpose very well, but is numerically very expensive. This work extends the very efficient Büttiker probe concept to phonon NEGF and discusses all implications of this method. Büttiker probe parameters are presented that reproduce within NEGF experimental phonon conductances of Si and Ge between 10K and 1000K. Results of this method in Si/Ge heterojunctions illustrate the impact of interface relaxation on the device heat conductance and the importance of inelastic scattering for the phonon distribution.

I. INTRODUCTION

State of art semiconductor logic and optoelectronic devices such as nanotransistors, quantum well photodetectors, and cascade lasers have characteristic device dimensions within the nanometer length scale^{1,2}. All of these devices face intense Joule heating and phonon dissipation during their operation. Well established methods to describe the phonon transport are either solving the Boltzmann transport equation (BTE)^{3,4} or the molecular dynamics^{5,6}. On the nanometer length scale, however, these methods miss important quantum physics such as tunneling, confinement and interference effects⁷⁻⁹. For Fermionic nanoscale transport such as transport of charge and spin, the nonequilibrium Green's function method (NEGF) has proven to consistently and accurately describe coherent and incoherent quantum effects^{10,11}. For phonon transport the NEGF method was predominantly used in the coherent (i.e. ballistic) approximation¹²⁻¹⁶. This is mainly due to the fact that scattering in NEGF typically requires self-consistent iterations of the NEGF equations. Such iterative solutions (called “self-consistent Born approximation”) are numerically very demanding both in memory and CPU time which typically prevents applications to concrete, atomically resolved nanostructures. The work of Ref.17 and Ref.18 are rare exceptions of this trend. The numerical load of self-consistent Born approximations is known to be high for electronic NEGF as well. This motivated Büttiker et al. to introduce an efficient heuristic scattering model for electronic transport in NEGF which is commonly called “Büttiker probes”^{19,20,21}. This model allows direct fitting to experimental transport data while avoiding self-consistent iterations within the NEGF equations¹⁷.

In this work, the Büttiker probe model is expanded to cover incoherent scattering in the atomistic phonon NEGF implementation of the nanodevice simulation tool NEMO5²². The phonon Büttiker probe model is setup to mimic the frequency and temperature dependence of the phonon scattering rates and the material-specific heat conductance established for silicon and germanium in the BTE method. The physics behind this phonon Büttiker probe model is illustrated and discussed for a fictitious material with varying the effective scattering strength. The relevance of quantum transport with phonon relaxation is demonstrated with resonant phonon transport in a quasi-one dimensional Ge/Si heterostructure.

II. METHOD

All silicon and germanium phonons in this work are represented in the modified valence force field model (MVFF) of Ref.23 and Ref.24. This MVFF model for silicon and germanium includes the coupling energies of atoms coupled with their first and second nearest neighbors in the material volume and third nearest neighbors in the plane of the first and second neighbors (i.e. third nearest neighbor coplanar coupling). All MVFF parameters are taken from Ref.23. Parameters at Si/Ge interfaces are arithmetical averages of the Si and Ge volume parameters. Based on the potential energy U and the harmonic approximation, the dynamical matrix (D) is calculated as

$$D_{mn}^{ij} = \frac{\partial^2 U}{\partial r_m^i \partial r_n^j}, \quad i, j \in N_A \text{ and } m, n \in [x, y, z], \quad (1)$$

with N_A the number of atoms in the active device, r_m^i and r_n^j the coordinates of atoms i and j , and x, y , and z the three different spatial directions. If not stated otherwise, Si/Ge interfaces are relaxed to minimize the potential energy U .

The nonequilibrium Green's function method requires the solution of a set of partial differential equations which read for the case of phonons^{15,17,20}:

$$G^R(E) = [E^2 - D - \Sigma_{\text{contact}}^R - \Sigma_{\text{BP}}^R]^{-1}, \quad (2)$$

$$G^<(E) = G^R [\Sigma_{\text{contact}}^< + \Sigma_{\text{BP}}^<] G^{R\dagger}, \quad (3)$$

where $\Sigma_{\text{contact}}^R = \Sigma_{\text{left}}^R + \Sigma_{\text{right}}^R$, is the sum of the contact self-energies representing the device's connection to the left and right phonon reservoir at the device/lead interface¹⁰. In stationary calculations of nanowires, Green's functions and self-energies are depending on the phonon energy E only. For periodic devices (e.g. ultrathin body UTB transistors) each assumed periodic boundary condition perpendicular to transport contributes an additional momentum to the parameter list of Green's functions and self-energies. For a given parameter set (e.g. a given energy and momentum in UTB transistors), Green's functions and self-energies are matrices in the propagation degrees of freedom of the active device: e.g. if the device is discretized with 1000 atoms, the numerical matrices are discretized with 3000 degrees of freedom. It is common to assume

for the “lesser-than” contact self-energy $\Sigma_{\text{contact}}^<$ that phonons in the leads are given in equilibrium Bose distribution functions:

$$\Sigma_{\text{contact}}^< = \frac{1}{e^{E/k_B T_{\text{left}}-1}} (\Sigma_{\text{left}}^{\text{R}} - \Sigma_{\text{left}}^{\text{R}\dagger}) + \frac{1}{e^{E/k_B T_{\text{right}}-1}} (\Sigma_{\text{right}}^{\text{R}} - \Sigma_{\text{right}}^{\text{R}\dagger}) \quad (4)$$

with the temperature T_{left} and T_{right} of the left and right phonon reservoir, respectively. The incoherent scattering of phonons is represented with one Büttiker probe self-energy per degree of freedom in the device

$$\Sigma_{\text{BP}(i,m)}^{\text{R}} = -i \frac{2\omega}{\tau}, \quad (5)$$

$$\Sigma_{\text{BP}(i,m)}^< = \frac{1}{e^{E/k_B T_{(i,m)}-1}} \Sigma_{\text{BP}(i,m)}^{\text{R}}, \quad (6)$$

with τ , the scattering life time and $T_{(i,m)}$, the temperature of the Büttiker probe at atom i and phonon polarization m . The retarded scattering self-energy is also included in the retarded contact self-energy calculation, following Refs. [17,25]. The retarded scattering self-energy is chosen to represent phonon-phonon Umklapp scattering $\tau_{p-p}^{-1} = C\omega^2 T^\alpha$, impurity scattering $\tau_{IM}^{-1} = B\omega^4$, and grain boundary scattering $\tau_b^{-1} = v_s/LF$ in the relaxation time approximation^{4,26,27}. The total relaxation time is additive so that $\tau^{-1} = \tau_b^{-1} + \tau_{IM}^{-1} + \tau_{p-p}^{-1}$. Here, τ_b , τ_{IM} and τ_{p-p} are the relaxation times for the grain boundary scattering, impurity scattering and phonon-phonon Umklapp scattering, respectively. The grain boundary scattering rate is determined by the average phonon velocity v_s , the Casimir boundary length L , and a geometry factor F all taken from Ref. [4]. The scattering on impurities τ_{IM}^{-1} and on other phonons τ_{p-p}^{-1} depends on B , C , and α , respectively. Here, B , C , and α are chosen to best reproduce the thermal conductivity of silicon and germanium of Refs. [4,28]. The general temperature dependence of phonon-phonon scattering requires to have a temperature dependent (see Table I)

TABLE I. Fitting parameters for the Büttiker probes in Eq.(5)

Material	$B(s^3)$	$C(sK^\alpha)$	α
Si	0.71×10^{-45}	1.74×10^{-21}	1.64
Ge	3.2×10^{-45}	1.12×10^{-20}	1.48

The temperature of each Büttiker probe $T_{(i,m)}$ is solved iteratively with the Green’s functions via the Newton’s method [22] until the integrated energy current

$$I_{(i,m)} = \int_{-\infty}^{+\infty} \sum_{j=1, j \neq i}^{N_A} \sum_{n=1, n \neq m}^3 \frac{1}{h} E \left[\mathcal{T}_{(i,m)(j,n)}(E) \left(\frac{1}{e^{E/k_B T_{i.m}-1}} - \frac{1}{e^{E/k_B T_{j.n}-1}} \right) + \mathcal{T}_{(i,m)\text{left}}(E) \left(\frac{1}{e^{E/k_B T_{i.m}-1}} - \frac{1}{e^{E/k_B T_{\text{left}}-1}} \right) + \mathcal{T}_{(i,m)\text{right}}(E) \left(\frac{1}{e^{E/k_B T_{i.m}-1}} - \frac{1}{e^{E/k_B T_{\text{right}}-1}} \right) \right] dE \quad (7)$$

vanishes for each Büttiker probe (i,m) . Here, $\mathcal{T}_{(i,m)(j,n)}$, $\mathcal{T}_{(i,m)\text{left}}$ and $\mathcal{T}_{(i,m)\text{right}}$ are the transmission functions between

Büttiker probe (i,m) and (j,n) , and the left and right reservoir, respectively²⁰. If not stated otherwise, all results in this work include the phonon scattering on grain boundaries, impurities and other phonons. Note that Eq.(7) is correct only for nanowire devices. If the considered device contains periodic directions, the transmission functions depend on the respective momenta. Then, the integral in Eq.(8) includes those momenta as well. This scattering model of Eqs.(5-7) is equivalent to the electronic Büttiker probe model of Ref. [20]. It implies that the limit for the phonon thermalization at each degree of freedom in the device (i.e. for each atom and each polarization direction) agrees with the respective local Büttiker probe temperature. The actual local temperature can differ from the Büttiker probe one depending on the transport situation. An estimate of the local temperature can be extracted from the average phonon gas energy

$$\langle E \rangle = \int E^2 G^<(E) dE \approx \int E^2 \frac{A}{e^{E/k_B T_{local}} - 1} dE. \quad (8)$$

where A is the spectral function $A = i(G^R - G^{R\dagger})$. In this way, an effective, locally thermalized phonon gas of temperature T_{local} is assumed that matches the phonons solved in the NEGF equations with respect to their average energy. The average phonon mean free path λ can be extracted following Ref. [29].

III. RESULTS

Figure 1 compares the experimental thermal conductivity of silicon and germanium of Refs.[4,28] with the scattered NEGF results of Eqs.(2-8). The fit of the scattering parameters in Table 1 allow the NEGF method to reproduce the thermal conductivity very well over a large temperature range. The inset of Fig. 1 shows the average phonon mean free path of silicon and germanium. The mean free paths at 300K are 130nm and 40nm for silicon and germanium, respectively, which agrees well with results in Refs. [7,30].

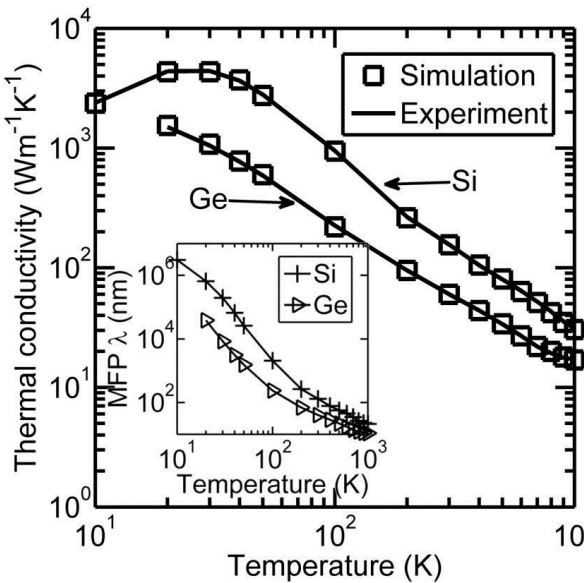


Figure 1. Calculated and experimental [4,28] thermal conductivity in [100] direction as a function of temperature for Si and Ge. The Büttiker probe parameters in Table 1 are fit to get a good agreement of the numerical data with experiment. The inset shows the mean free path corresponding to the conductivity.

Figures 2 compare the Büttiker probe temperatures with the local temperature T_{local} of Eq.(9) in 5.3nm homogeneous silicon in between two leads of 305K (left reservoir) and 300K (right reservoir) phonon temperature, respectively. Here, the Büttiker probe temperatures are averaged over the 3 polarization directions m as a function of the atom position along the transport direction $\sum_{m=1}^3 T_{(i,m)}/3$. It is worth to note that the polarization dependence of the Büttiker probe temperature depends on scattering strengths and phonon dispersions. By construction, the Büttiker probe temperature is the target temperature of the phonon thermalization processes in the device. The local temperature T_{local} of Eq.(9) is polarization independent by definition. To illustrate the impact of different scattering strengths, the calculations in Figs. 2 include only the phonon-phonon scattering with varying scattering amplitude. It is shown in Figs.2 that the stronger the scattering, the larger is the temperature drop within the device and consequently the smaller is the phonon conductance. The temperature drops close to the lead/device interfaces are more pronounced with larger heat conductivities. This effect is similar to the depletion effects discussed already in the area of electronic transport^{25,31-33}. The larger the heat flow in the device is, the larger is the average velocity of the phonon gas in the device. Since equilibrium distributions are assumed in both leads, the phonons that enter (leave) the device at the left (right) device boundary need to get accelerated (decelerated). The acceleration causes a phonon depletion and the deceleration a phonon accumulation close to the leads. Accordingly, the phonon temperatures on the device side of the lead/device interfaces differ from the assumed lead temperatures. Alternative lead models that assume drifted distribution functions^{25,32} or a change in the number of phonons/particles in the leads³⁴ give smaller temperature drops at the lead/device interface.

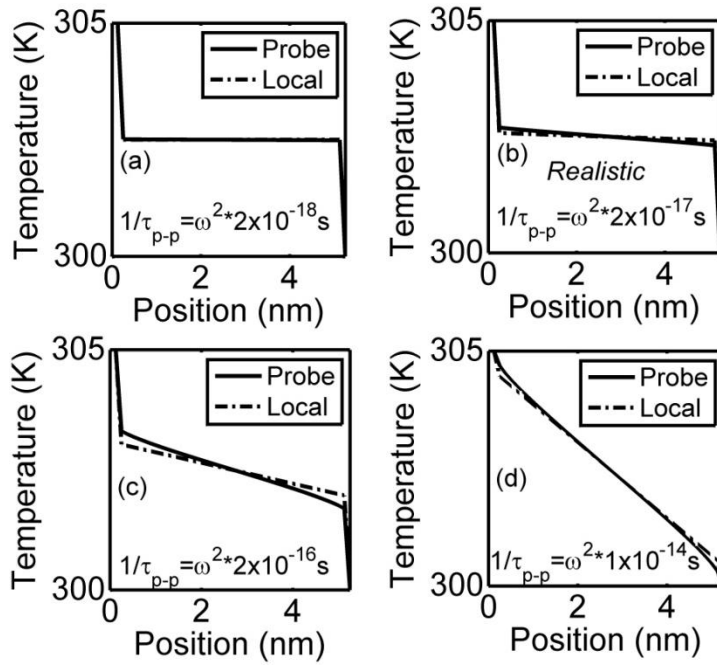


Figure 2. Calculated local and Büttiker probe temperature in homogeneous 5.8 nm thick Si between Si leads of 305K and 300K when only phonon-phonon scattering is included and the phonon scattering prefactor is varied. The transport direction is along the [100] crystal axis. Quasi ballistic (a) and realistically scattered (b) transport calculations show almost constant local temperature. Transport calculations with 10x (c) and 50x (d) larger than realistic scattering show pronounced temperature drops over the device.

Figure 3 shows the local temperature profile in several nanometers around a Si/Ge interface for various scattering strengths. Similar to Figs.2, the left and right reservoir temperatures are 305K and 300K, respectively. Similar to Figs.2, the larger the scattering of the phonons in the bulk materials, the more temperature drops in the material's volume and the smaller is the temperature drop across the actual Si/Ge interface.

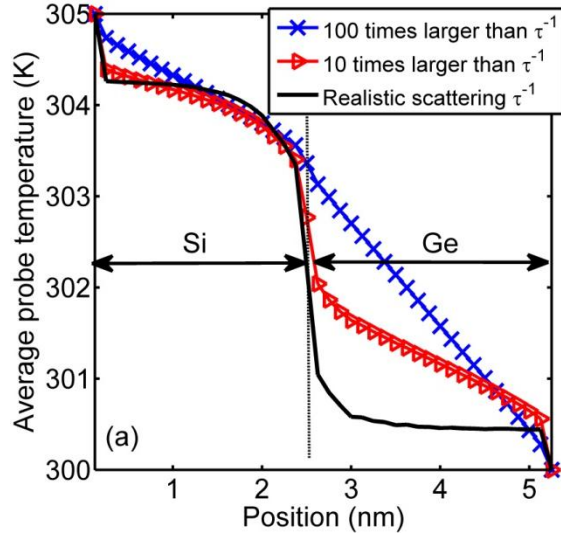


Figure 3. Local temperature of a silicon/germanium interface connected to homogeneous semi-infinite Si and Ge leads of 305K and 300K phonon temperature, respectively. The transport direction is along [100] crystal direction. The scattering rates of Si and Ge are varied with constant factors (10x triangles, and 100x crosses) in Si and Ge simultaneously.

Atoms at and close to Si/Ge interfaces have to relax from their native Si and Ge crystal positions to minimize the lattice energy. It is important to include this relaxation in the thermal transport calculation as shown in Fig. 4. The phonon conductance of the relaxed Si/Ge interface of Figs.3 with realistic scattering rates in Si and Ge is about 10% higher than in the scenario with all atoms on the native Ge lattice. The impact of relaxation on the conductance reduces with larger scattering rates in Si and Ge as also shown in Fig.4. Here, the ratio between the scattering rates in Si and Ge is kept constant while the scattering strengths are varied with a scaling factor F. It is worth to mention that similar results were seen for 2-interface systems such as a thin Si layer embedded in semi-infinite Ge leads.

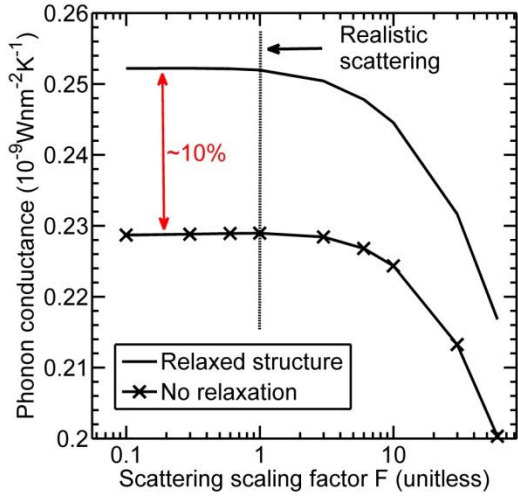


Figure 4. Phonon thermal conductance of the Si/Ge interface of Fig.3 with realistic scattering potentials scaled with a factor F for both Si and Ge simultaneously. The thermal conductance of the strain relaxed interface exceeds the conductance when all atoms are fixed on a Ge native lattice.

It is well known in electron transport that inelastic scattering is essential to fill confined states^{1,35}. This also holds for phonon transport as illustrated in Figs.5 for a 3nm Ge layer embedded in between 2 3nm thick Si layers and Ge leads with 305K and 300K for the left and right lead temperature, respectively. Figures 5 compare the energy resolved phonon density solved in ballistic NEGF (a) and in scattering NEGF (b) with the Büttiker probe parameters of table 1. Ballistic calculations underestimate the amount of central-layer phonons. Only lowest energy acoustic phonons tunnel into the central Ge layer and contribute to the phonon density. Phonons of higher energies either get into the central Ge layer by scattering supported tunneling through the Si layers or by tunneling of low-energy phonons and subsequent energy absorption within the central Ge layer. Note that the phonon modes of the thin Si layers hardly couple to the Ge leads in the relevant energy range. Consequently, there are hardly any phonons in the Si layers. Similar findings of quantum phonon transport in nanowire heterostructures were reported in Ref. [17]. Note that the ratio of phonon conductance predicted in ballistic ($7.43\text{WK}^{-1}\text{nm}^{-2}$ in Fig.5 (a)) and scattering NEGF ($7.29\text{WK}^{-1}\text{nm}^{-2}$ in Fig5 (b)) depends in general on device details.

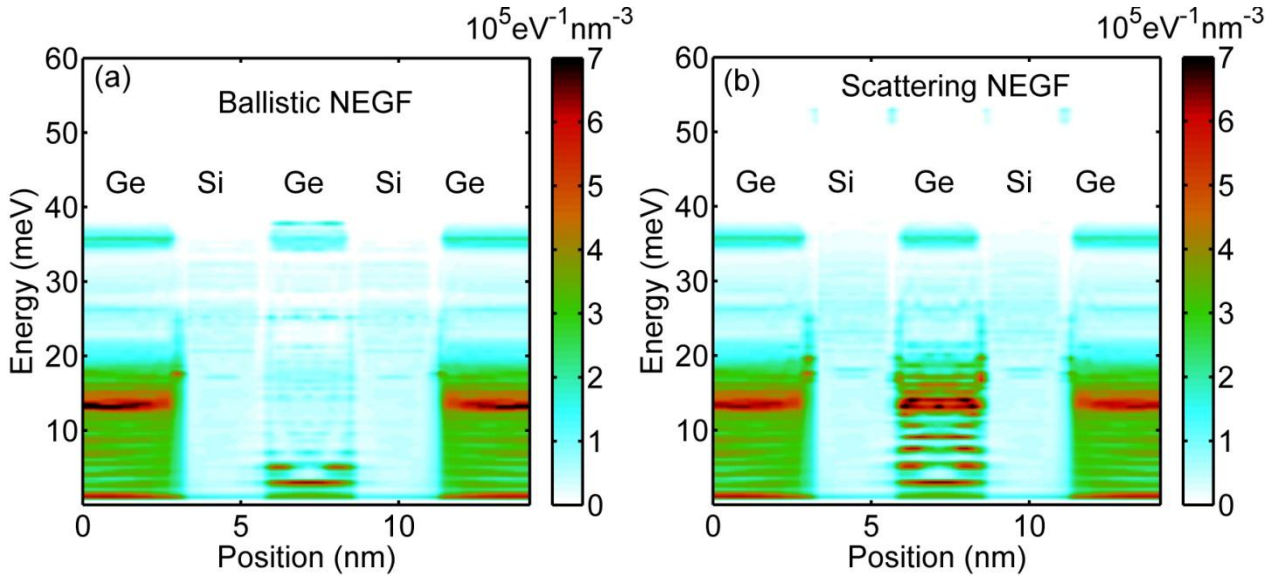


Figure 5. Energy resolved phonon density of a 3nm Ge layer separated by 2 3nm Si layers from semi-infinite homogeneous Ge. The right and left lead temperature is 305K and 300K, respectively. All layers are [100] orientated. The central Ge layer shows less phonon density in the ballistic case (a) compared to the calculation including inelastic scattering (b).

IV. CONCLUSION

In conclusion, the heuristic scattering quantum transport method of NEGF with Büttiker probes is extended from the electronic framework to phonon transport. The scattering parameters of Büttiker probes in Si and Ge are fit to reproduce the experimental thermal conductance data. The temperature drop across Si/Ge interfaces is the more pronounced, the larger the phonon conductance in homogeneous Si and Ge is, respectively. The relaxation of atoms at and surrounding interfaces of different crystals has a significant influence on the overall heat conductance. It is also illustrated how inelastic scattering can fill phonons into Ge layers across several nanometer thick Si barriers. Such Ge layers are predicted to be almost phonon-free in ballistic calculations.

ACKNOWLEDGEMENTS

REFERENCES

- ¹C. Jirauschek and T. Kubis, *Appl. Phys. Rev.* 1, 011307 (2014).
- ²T. Kubis, S. Mehrotra, and G. Klimeck, *Appl. Phys. Lett.* 97, 261106 (2010).
- ³J. Callaway, *Phys. Rev.* 113, 1046 (1959).
- ⁴M. G. Holland, *Phys. Rev.* 132, 2461 (1963).
- ⁵A. J. Minnich, M. S. Dresselhaus, Z. F. Ren, and G. Chen, *Energy Environ. Sci.* 2, 466 (2009).
- ⁶Y. He and G. Galli, *Phys. Rev. Lett.* 108, 215901 (2012).
- ⁷J. Knoch, S. Mantl, and J. Appenzeller, *Solid-State Electronics* 51, 572 (2007).
- ⁸S. O. Koswatta1, D. E. Nikonorov, and M. S. Lundstrom, *IEDM Tech. Dig.* 525 (2005).
- ⁹A. Matyas, T. Kubis, P. Lugli, and C. Jirauschek, *Physica E* 42, 2628 (2010).
- ¹⁰S. Datta, *Electronic Transport in Mesoscopic Systems* (Cambridge University Press, Cambridge, 1995).
- ¹¹R. Zen, R. Venugopal, S. Goasguen, S. Datta, and M. S. Lundstrom, *IEEE Trans. Electron Devices* 50, 1914, 2003.
- ¹²N. Mingo and L. Yang, *Phys. Rev. B* 68, 245406 (2003).
- ¹³T. Yamamoto and K. Watanabe, *Phys. Rev. Lett.* 96, 255503 (2006).
- ¹⁴W. Zhang; T. Fisher; and N. Mingo, *Journal of Heat Transfer* 129, 483 (2007).
- ¹⁵Z. Tian, K. Esfarjani, and G. Chen, *Phys. Rev. B* 89, 235307(2014).

¹⁶T. Markussen, A. Jauho, and M. Brandbyge, Phys. Rev. B 79, 035415 (2009).

¹⁷M. Luisier, Phys. Rev. B 86, 245407 (2012).

¹⁸J. Wang, B. K. Agarwalla, H. Li, J. Thingna, Front. Phys. 9, 673 (2014).

¹⁹M. Büttiker, Phys. Rev. Lett. 57, 1761 (1986).

²⁰R. Venugopal, M. Paulsson, S. Goasguen, S. Datta, and M. S. Lundstrom, J. Appl. Phys. 93, 5631 (2003).

²¹P. Greck, S. Birner, B. Huber, and P. Vogl, Opt. Express 23, 6587 (2015).

²²J. E. Fonseca, T. Kubis, M. Povolotskyi, B. Novakovic, A. Ajoy, G. Hedge, H. Ilatikhameneh, Z. Jiang, P. Sengupta, Y. Tan, and G. Klimeck, J. Comput. Electron 12, 592 (2013).

²³A. Paul, M. Luisier, G. Klimeck, J Comput. Electron 9, 160 (2010).

²⁴S. Steiger, M. Salmani-Jelodar, D. Areshkin, A. Paul, T. Kubis, M. Povolotskyi, H.-H. Park, and G. Klimeck, Phys. Rev. B 84, 155204 (2011).

²⁵T. Kubis and P. Vogl, Phys. Rev. B 83, 195304 (2011).

²⁶M. Asen-Palmer, K. Bartkowski, E. Gmelin, M. Cardona, A. P. Zhernov, A. V. Inyushkin, A. Taldenkov, V. I. Ozhigin, K. M. Itoh, and E. E. Haller, Phys. Rev. B 56, 9431 (1997).

²⁷P. G. Klemens, Proc. Phys. Soc. London A68, 1113 (1955).

²⁸C. J. Glassbrenner, G. A. Slack, Phys. Rev. 134, 1058 (1964).

²⁹M. S. Lundstrom, IEEE Elec. Dev. Lett. 22, 293 (2001).

³⁰C. Jeong, S. Datta, and M. Lundstrom, J. Appl. Phys. 111, 093708 (2012).

³¹S. Datta, Superlattices and Microstructures 28, 253 (2000).

³²W. R. Frensley, Rev. Mod. Phys. 62, 745 (1990).

³³W. Pötz, J. Appl. Phys. 86, 2458 (1989).

³⁴J. Maassen and M. Lundstrom, J. Appl. Phys. 117, 035104 (2015).

³⁵J. Guo, J. Appl. Phys. 98, 063519 (2005).